



**HAL**  
open science

## Modeling the squeezed-thin film using generalized oedometric Reynolds equations

Van-Vuong Lai, Emilie Delplanque, Francois Sidoroff, Denis Mazuyer, Juliette Cayer-Barrioz

► **To cite this version:**

Van-Vuong Lai, Emilie Delplanque, Francois Sidoroff, Denis Mazuyer, Juliette Cayer-Barrioz. Modeling the squeezed-thin film using generalized oedometric Reynolds equations. Tribology International, 2023, 186, pp.108558. 10.1016/j.triboint.2023.108558 . hal-04119822

**HAL Id: hal-04119822**

**<https://hal.science/hal-04119822>**

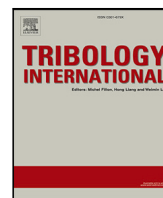
Submitted on 6 Jun 2023

**HAL** is a multi-disciplinary open access archive for the deposit and dissemination of scientific research documents, whether they are published or not. The documents may come from teaching and research institutions in France or abroad, or from public or private research centers.

L'archive ouverte pluridisciplinaire **HAL**, est destinée au dépôt et à la diffusion de documents scientifiques de niveau recherche, publiés ou non, émanant des établissements d'enseignement et de recherche français ou étrangers, des laboratoires publics ou privés.



Distributed under a Creative Commons Attribution - NonCommercial - NoDerivatives 4.0 International License



# Modeling the squeezed-thin film using generalized oedometric Reynolds equations

Van-Vuong Lai, Emilie Delplanque, Francois Sidoroff, Denis Mazuyer, Juliette Cayer-Barrioz \*

Laboratoire de Tribologie et Dynamique des Systemes, CNRS UMR 5513, Ecole centrale de Lyon, 36 avenue guy de collongue, F-69134, Ecully, France

## ARTICLE INFO

### Keywords:

Numerical simulation  
Adsorbed nanometric boundary layers  
Mechanical properties  
Squeeze film  
Interfacial hydrodynamics

## ABSTRACT

The behavior of confined flows at the nanometer scale remains largely unpredictable, especially when hydrodynamic separation is of the same order of magnitude of the surface roughness. Here we propose a continuum mechanics-based model integrating solid deformation, fluid compressibility and solicitation frequency to capture and predict the squeeze of a heterogeneous confined thin film between two nanometer-thin antagonistic adsorbed layers on solid surfaces, in both static and dynamic oscillating situations. Validated by direct confrontation to theoretical and experimental results, this model allowed us to provide physical insights in the squeeze mechanisms, confirming the role of the fluid compressibility at the onset of contact, discussing the influence of the adsorbed layer shear elastic modulus for instance, and defining a viscosity-frequency equivalence. It also permitted to assess the mechanical properties of the nanometer-thin adsorbed layers in both situations, when separated by a fluid film and when in contact.

## 1. Introduction

The control and the understanding of confined flows at the nanometer scale are of prior importance in the problem of lubrication that raises the question of stress transmission at a solid interface through a thin liquid film. Because of the increasing use of low-viscosity fluids, the hydrodynamic separation reaches the order of magnitude of the solid surface roughness. Literature has therefore focused on friction modifier additives adsorbed onto the surfaces where they form nanometer-thick layers, and their role in the friction mechanisms (see for instance [1–7]). Their structural and chemical properties have been characterized thanks to the development of various advanced experimental techniques, among others Neutron reflectometry [8], Atomic Force Microscope (AFM) and Surface Force Apparatus (SFA) [9] and its derived techniques [10–12]. For instance, [6] showed the existence of 1.6-nm-thick adsorbed layer of palmitic acid on smooth iron oxide surfaces; [13,14] detected irregular islands of stearic acid on mica surfaces and [2,15] evidenced the influence of polymeric layers adsorbed on the surfaces on drainage properties. Moreover, the rheology of the boundary layers formed by the interactions between the lubricant molecules and the surfaces is a key parameter both in the friction control and in the full-film forming capability of contacts. The presence of these thin molecular layers at the extreme surface also modifies the overall interfacial shearing as well as the slip conditions at the wall.

However, the first approaches relied on the assumption of no-slip boundary conditions. For instance, for the modeling of the drainage

of a confined film between two solids, Chan and Horn [16] applied Reynolds's equation to a system consisting of two cylinders separated by a homogeneous Newtonian viscous fluid. Assuming that there is no deformation of the substrates and neglecting both gravitational and inertial contributions, the film can be fully characterized using its damping behavior as a function of the separation distance and the fluid viscosity. Hadzioannou and Montfort [17] then generalized Chan and Horn's model [16] to the case of an incompressible viscoelastic fluid. With this model, the film has both stiffness and damping behavior depending on its shear elastic modulus. More sophisticated modeling have then been proposed, some of them taking the surface deformation into account. For instance, in the case of a sphere/plane contact, Auslender *et al.* [18] developed an analytical model considering an elastic fluid film confined between two surfaces. The key role of the film compressibility was highlighted, leading to the development of a oedometric thin film model. Later, Trifa *et al.* [19] extended the generalized oedometric Reynolds model [18] to take the elastic substrates into account. Recently, Movchan *et al.* [20] presented accurate asymptotic solutions using the principle of Saint-Venant for the axisymmetric deformation of thin films constrained by two rigid solids. The solutions are valid in the whole range of Poisson's ratio, and make it possible to distinguish compressible, nearly incompressible and incompressible films.

These models perfectly describe the behavior of a homogeneous fluid film during squeeze, assuming no-slip conditions. However, in the

\* Corresponding author.

E-mail address: [juliette.cayer-barrioz@ec-lyon.fr](mailto:juliette.cayer-barrioz@ec-lyon.fr) (J. Cayer-Barrioz).

## Abbreviations

$x, y, z$	Cartesian coordinates
$r, \theta$	Polar coordinates
$R$	Sphere radius
$E'$	Reduced Young's modulus
$\eta$	Fluid viscosity
$K_f$	Bulk modulus of the fluid
$G_f$	Shear modulus of the fluid
$K_c$	Bulk modulus of the adsorbed layer
$G_c$	Shear modulus of the adsorbed layer
$M_{od}$	Oedometric modulus
$E, \nu$	Young modulus and Poisson ratio
$h$	Surface separation distance
$\delta D$	Imposed displacement of the sphere
$F_n$	Static contact force
$\Re(\bullet)$	Real part of $\bullet$
$\Im(\bullet)$	Imaginary part of $\bullet$
$K_z$	Dynamic interface stiffness
$Im_z$	Dynamic interface damping
$\omega$	Pulsation of imposed displacement oscillation
$\sigma, u$	Stress and displacement of confined film
$w_r$	Relative elastic deformation of solid surfaces in the contact zone
$a, \delta$ and $\sigma_o$	Contact zone radius, static penetration and normal stress obtained by Hertz theory
$Z$	Nominal position of the sphere to the plane without solid deformation at the center $r = 0$
$D_o$	Adsorbed layer thickness
$L_H$	Thickness of the "immobile" layer on each surface
$\sigma_n$	Hertzian contact pressure
$\sigma_o$	Maximum Hertzian contact pressure
$V_z$	Velocity of the sphere towards the plane in the vertical direction

case of the drainage of more complex fluid with adsorbed species on the surfaces or in the case of squeeze including surface deformations, numerous experimental works [2,4,15,21,22] highlighted large discrepancies with these theories. These discrepancies result from a structural heterogeneity in the confined film, such as:

- the existence of an adsorbed homogeneous layer of simple molecules [21,23], considered of infinite viscosity, that shifts the no-slip boundary conditions to a distance  $2D_o$ , with  $D_o$  corresponding to the thickness of the immobile layer on each surface, immobile layer which do not participate to the hydrodynamic flow. Moreover, a viscoelastic behavior of the layer not only induces a divergence in the damping evolution compared to the theoretical one, but also leads to a divergence in the overall stiffness behavior, especially at a short distance between solid surfaces.
- the existence of an adsorbed layer of polymers, with a gradient of viscous properties [2], that shifts the no-slip boundary conditions and induces a divergence in the damping evolution compared to the theoretical one. In addition, the gradient of viscous properties is not sufficient to explain the increase in stiffness at a short distance between two facing solid surfaces.

Attempts to account for the existence of these boundary layers on the surface were theoretically made by Tonck [10], Auslender [24]

for rigid surfaces and later, numerically, by Trifa [25] for compliant surfaces. Tonck [10] proposed an annular model based on the superposition of parallel assembly of different local rheological models defined on elementary rings while Auslender [24] and Trifa [25] models based on the generalized oedometric Reynolds model [18]. Without direct interaction between the sphere and supported films, to measure the mechanical properties of adsorbed layer, Leroy *et al.* [26] used the elasto-hydrodynamic (EHD) interaction of a sphere with a flat elastic surface. This method consists in applying the lubrication equation [27] for the drainage flow of the fluid between the sphere and the plane using the Green function as the zeroth-order Hankel transforms for the relationship between the normal displacement of adsorbed layer on the flat and the contact pressure [28]. They were then able to establish a phase diagram of the EHD interaction which defines different behaviors of the resulting contact force response in order to optimize experimental conditions. These above-mentioned models allowed one to measure the mechanical properties of micrometer-thick adsorbed layers for large separation distances without contact between adsorbed layers. Nevertheless, according to the phase diagram of the EHD interaction [26], the transition from the viscous regime to the elastic one depends on the thickness of adsorbed layer. When dealing with a very thin adsorbed layer at a nanometric scale, it requires a much smaller distance between the sphere and layer. This reduces the efficiency of these without-contact SFA measurements. In addition, this model was limited to the case of purely elastic film and homogeneous fluid. Therefore, it cannot predict experimental situations with viscoelastic films and heterogeneous fluid as observed in the literature (see [22] for instance).

Furthermore, the above-mentioned models cannot monitor the evolution of the contact quantities or mechanical properties of adsorbed layers when contact between layer/layer or layer/solid occurs. One of the main additional issues in modeling the squeeze behavior taking into account the existence of an adsorbed layer is the question of the onset of static contact between these molecular thin layers when the surfaces start interacting. Some authors [4,5,23,29] considered in a first approximation that no deformation of these molecular layers take place due to a high surface coverage inducing high compressibility of the adsorbed layer under pressure. The substrate deformation could then be determined using a non-adhesive (typically Hertz') or an adhesive (JKR or DMT's) theory depending on the associated experimental measurements. However, the important role of film compressibility and substrate deformation cannot be ignored, especially for a thin film as highlighted in [19,24,30]. Thus, in these works, to model the contact between the two adsorbed layers, they assumed a hyper-elastic behavior of these boundary layers using a Mooney–Rivlin-like energy in which a term of compressibility was added. They obtained very different rheological properties of the layers in a static contact analysis compared to those obtained in a dynamic analysis, under small oscillations, using the generalized oedometric Reynolds model [24]. This discrepancy was attributed to the use of independent solving methods for the static and dynamic analysis.

Various numerical methods can indeed be implemented to model the interactions of two coated surfaces. The JKR theory [31] was extended to the case of thin layers by semi-analytical methods [32,33] where the coating response associates the zeroth-order Hankel transforms of the normal displacement to the contact pressure [28]. Besides, the finite element method (FEM) is widely used [34–38]. To overcome the highly expensive time computation using FEM, some authors [39–41] also solved the problem by finding analytically coefficients which link the contact stress and displacements. These coefficients were converted from the elastic field solution in the frequency domain, by using a conversion method based on the fast Fourier transform. Iterative methods have been often used when the contact region is not known in advance. However, when the Young modulus of the nanometric layer is much smaller than that of the substrates (for instance a polymer film on a glass substrate), the convergence of the iterative resolution for

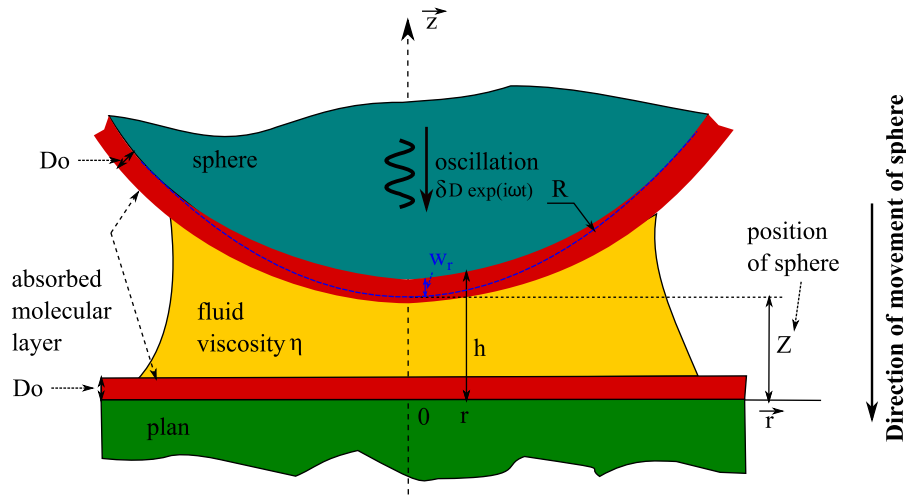


**Fig. 1.** Geometry of the squeeze of a thin fluid film of viscosity  $\eta$ , between a sphere and a plane, both covered with an adsorbed layer of thickness  $D_o$ .  $Z$  is the nominal distance between the supposedly undeformed solids at  $r = 0$ . This distance  $Z$  can be measured experimentally.  $R$  is the sphere radius.  $w_r(r)$  is the deformation of the solids with  $r$  the distance to the center in polar coordinates.

the nonlinear contact problem is not always ensured, especially for a nearly incompressible film [42]. Molecular dynamic (MD) simulations also predicted the adsorption of stearic acids and allowed to discuss the organization as a function of the amount of molecules/surface [43–46]. Atomic interaction forces between molecules were described using the DREIDING force field [47] or the Morse potential function [45]. The major drawbacks of molecular simulations are that the system has to operate for a limited number of molecules, on short-time scales and unrealistic approaching velocity between the two solids.

In this context, this paper aims at developing a numerical model based on continuum mechanics which fully simulates the squeeze of a heterogeneous confined thin film between two nanometric antagonistic adsorbed layers on solid surfaces. This model accounts for the film compressibility and the deformation of substrates in both static and dynamic situations. On the one hand, our model can predict quantities in the contact zone such as contact stress or complex stiffness. On the other hand, it provides physical insights of the squeeze mechanisms.

The manuscript is organized as follows. In Section 2, we describe the numerical model by presenting its formulation and the strategy developed to simultaneously solve the static and dynamic contact interactions. In Section 3, numerical results are validated by a direct confrontation to theoretical or experimental ones for model cases. Our model is then applied in Section 4 to investigate the influence of the mechanical properties of both adsorbed layers and fluid in both static and dynamic conditions in more complex situations. We also discuss the outcome in terms of coupling between the confined fluid and the surfaces.

## 2. Numerical model for the squeezed thin-film between elastic molecular layers adsorbed on solid surfaces

### 2.1. Description of the problem of a squeezed thin film between two solids

The problem of a squeezed fluid film between two solids (here, a sphere and a plane) is schematically illustrated in Fig. 1. A molecular layer of thickness  $D_o$  is adsorbed on each solid surface. The sphere can be moved towards and away from the plane in three directions ( $x$ ,  $y$ , and  $z$ ).

The distance between the two solid surfaces,  $h_s$ , can be classically written as:

$$h_s(r) = Z + \frac{r^2}{2R} + w_r(r) \quad (1)$$

where  $Z$  is the distance between the undeformed solids at  $r = 0$ .

Under harmonic oscillation of small amplitude, imposed on the sphere, the distance  $h(r, t)$  becomes:

$$h(r, t) = h_s(r) + \delta D e^{i\omega t} \quad (2)$$

where  $h_s(r, t)$  is the static sphere — plane distance,  $\delta D$  is the amplitude of imposed harmonic oscillation on the sphere and  $\omega$  is the oscillation pulsation.

The force  $F_n(t)$  generated by this movement is subsequently measured and decomposed into a static component  $F_s(t)$  and a dynamic one as follows:

$$F_n(t) = F_s + (\delta F' + i\delta F'')e^{i\omega t} \quad (3)$$

where  $\delta F'$  and  $\delta F''$  respectively represent the components in phase and in quadrature of phase of the dynamic force. These two components can be written in the form:

$$\begin{aligned} \delta F' &= K_z \delta D \\ \delta F'' &= Im_z \delta D \end{aligned} \quad (4)$$

where  $K_z$  and  $Im_z$  represent the stiffness and damping behavior of the interface respectively.

The force  $F_n(t)$  results from several contributions [21]: the wetting force due to the fluid meniscus, the contact forces due to the interactions between the solids (and/or the adsorbed layers) and the hydrodynamic force due to the flow of fluid between the sphere and the plane. Wetting and contact forces are both independent of the approaching velocity and contribute only to the static force. Here, we neglected both the wetting force variation due the size of the fluid meniscus, large compared to the contact and the hydrodynamic force. The calculation of the hydrodynamic force due to the fluid flow between the sphere and the plane, detailed in Appendix A, confirmed it could be neglected.

### 2.2. Generalized Reynolds model for the squeeze of a thin film between elastic molecular layers adsorbed on solid surfaces

Since the squeezed film is much thinner in comparison with the dimensions of the substrates, we adopted here the oedometric generalized Reynolds model developed in [24] and extended it to the case of solid deformation [19]. This model can be used for the squeezing of both compressible and incompressible films. We further extended this model to heterogeneous films, that is to say two adsorbed layers separated by a fluid film, during squeeze between elastic solids, at both large and small distances.

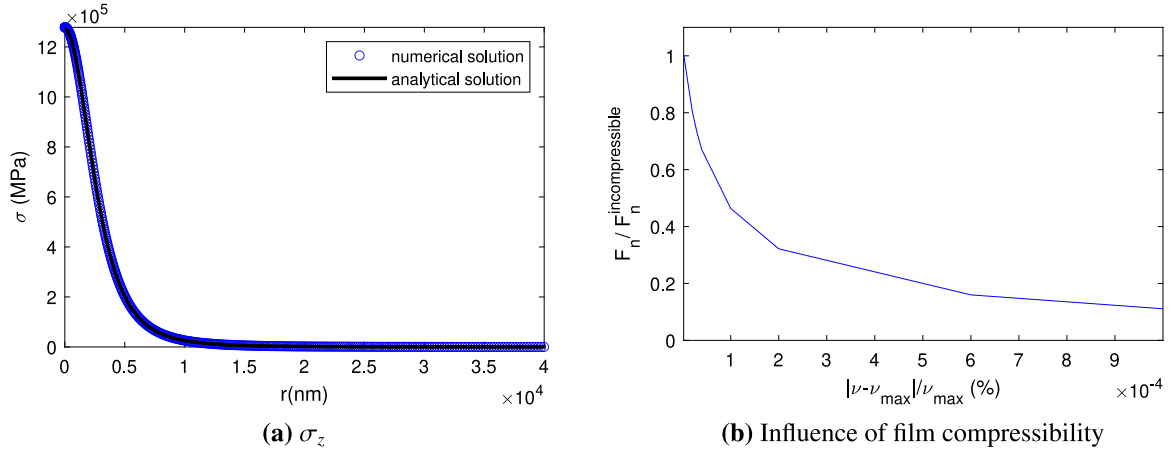


**Fig. 2.** (a) Normal stress distribution in the case of an incompressible interfacial layer squeezed between two rigid surfaces and (b) Influence of film compressibility. In (a) the numerical solution (dots) superimposes on the analytical one (line). Results in both figures were obtained with a shear modulus  $G = 10$  MPa,  $\delta D = 0.4$  nm,  $Z = 4.2$  nm,  $R = 1.94$  mm.

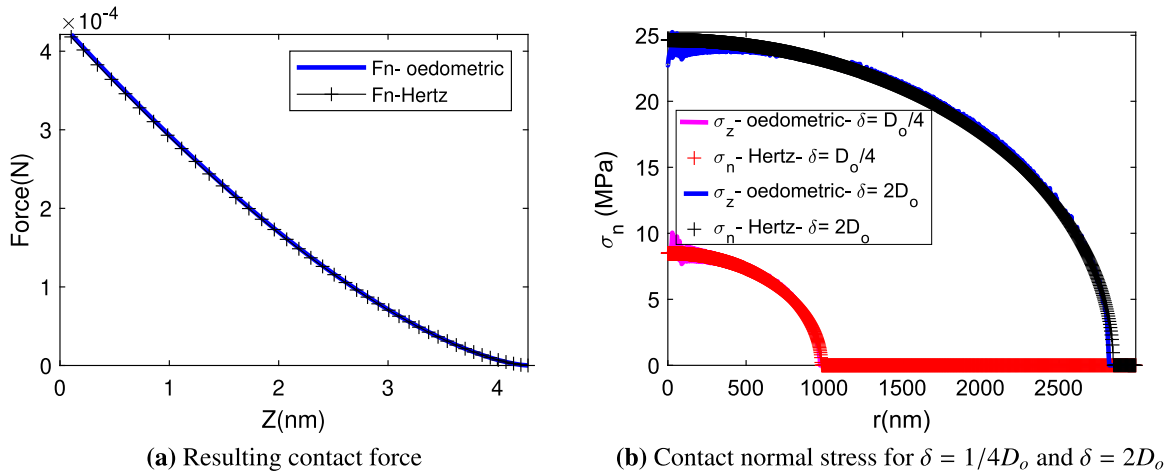


**Fig. 3.** (a) Resulting contact force evolution as a function of distance  $Z$  and (b) Normal stress distribution corresponding to two different static penetration  $\delta$ . The two identical layers of thickness  $D_o = 2.1$  nm have here the same mechanical properties as those of the solids. The layers were squeezed between a sphere of radius  $R = 1.94$  mm and a flat plane.

The squeezed interfacial film mechanical behavior was assumed to follow isotropic linear elastic Hooke's law, written as:

$$\sigma_{ij} = K \epsilon_{ii} \delta_{ij} + 2G e_{ij} \quad (5)$$

where  $K$  and  $G$  are respectively the bulk and the shear modulus.  $\epsilon_{ij}$  and  $e_{ij}$  denote the strain tensor and its deviator. The strain boundary conditions could be defined as:

$$\begin{cases} u = \delta D & \text{if } z(r) = h \\ u = 0 & \text{if } z(r) = 0 \end{cases} \quad (6)$$

To account for the existence of both the adsorbed molecular layers and the fluid, the interfacial film was considered as heterogeneous. Therefore, following the work of [18] on the oedometric Reynolds model, the stress tensor was written as a function of  $z$  as follows:

$$\sigma = \begin{Bmatrix} \gamma(z)\sigma_z & 0 & \tau_1 \\ 0 & \gamma(z)\sigma_z & \tau_2 \\ \tau_1 & \tau_2 & \sigma_z \end{Bmatrix} \quad (7)$$

where

$$\gamma(z) = \frac{K(z) - 2/3G(z)}{K(z) + 4/3G(z)}$$

As in [24,25], in the case of a very thin films, it was assumed that the vertical stress was independent of  $z$  and the terms  $\frac{\partial u_\alpha}{\partial z}$  were predominant in the calculation of the shear stresses. Assuming a relative elastic

substrate deformation,  $w_r$ , at small separation distance and following mathematical manipulations detailed in Appendix B, we obtained a partial differential equation in the cylindrical coordinate system:

$$C_o(r)\sigma_z(r) - \frac{1}{r} \frac{d}{dr} \left( r L_o(r) \frac{d\sigma_z}{dr} \right) = \delta D - w_r \quad (8)$$

where  $C_o$  and  $L_o$  are determined using Eqs. (B.6) and (B.14).

The resolution of Eq. (8) provided with the normal stress  $\sigma_z$ . The resulting contact force could then be determined as follows:

$$F_n = \int_0^R 2\pi\sigma_z(r)dr \quad (9)$$

### 2.3. Numerical steps for the resolution of the static contact between adsorbed molecular layers on the solid surfaces

The contact between the two adsorbed layers occurs when the distance  $h$  between two solid surfaces (Fig. 1) is smaller than the thickness  $2D_o$ . It was assumed that the static force  $F_s(t)$  only results from the contact between the two elastic molecular layers and the contribution of the fluid was neglected. The generalized Reynolds model was also adopted here. An explicit approach for the resolution of the static contact problem was chosen, based on small incremental displacement of the sphere towards the plan.

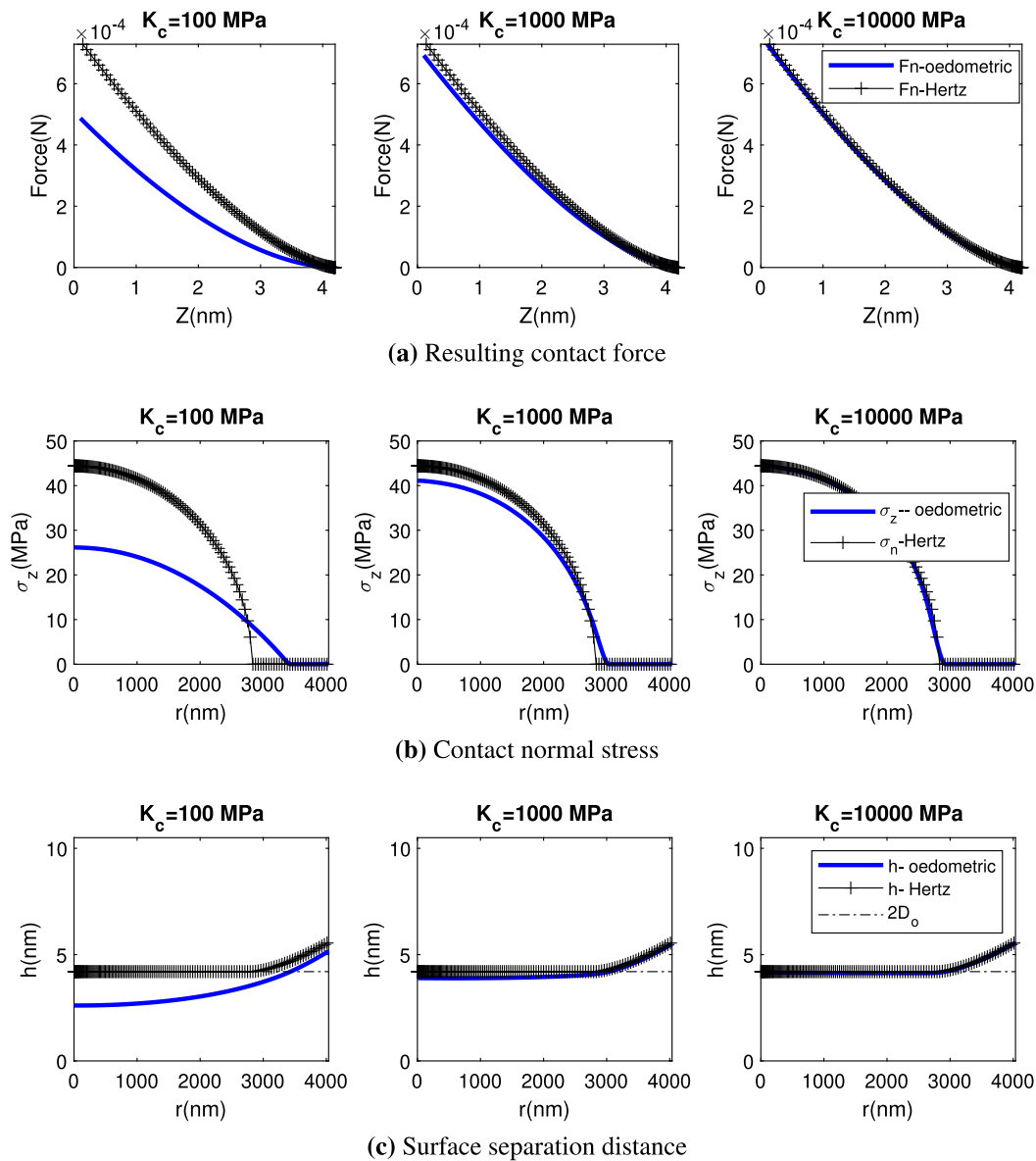


Fig. 4. Evolution of the resulting normal contact force as a function of distance  $Z$  (a), normal stress (b) and surface separation distance (c) corresponding to the maximal value of static force in the case of a static contact between two identical layers of thickness  $D_o = 2.1$  nm with a shear modulus  $G_c = 0.4$  MPa squeezed between a sphere of radius  $R = 1.94$  mm and a flat plane, numerical values taken from [4]. The effect of an increase of the bulk modulus, from  $K_c=100$  to 10000 MPa, can be seen from left to right.

The steps for the determination of the static solution are described below:

- In the *first step*, at the position  $z_i$  of the sphere, the contact was defined when the distance between the two antagonistic surfaces was smaller than the thickness of two molecular layers:

$$h_i \leq 2D_o$$

- In the *second step*, the imposed displacement is equal to  $\Delta D_s = z_{i+1} - z_i$ . For the considered small displacement, we used Eq. (B.24) to calculate the incremental stress  $\Delta\sigma_r$  and the relative displacement of solids is then determined using Eq. (B.21). In the case of heterogeneous film as shown in Eqs. (7), (B.6), (B.12) and (B.14), the displacement of the molecular layers can be determined using the oedometric assumption:

$$u(r, z) = \frac{\int_0^z 1/M_{od}(z)dz}{\int_0^{h_i} 1/M_{od}(z)dz} \Delta D_s(r)$$

where  $M_{od} = E \frac{1-\nu}{(1+\nu)(1-2\nu)}$  is the oedometric modulus (under oedometric conditions = vertical compression without lateral displacement).  $E, \nu$  are respectively the Young modulus and Poisson ratio of adsorbed layers.

- In the *third step*, the distance between the antagonistic surfaces was updated as follows:

$$h_{i+1} = h_i - \Delta D_s + \Delta w_r$$

#### 2.4. Extension to the harmonic sollicitation

It is noteworthy that the generalized Reynolds model presented in Section 2.2 was assumed still valid in the case with an harmonic sollicitation in agreement with [25,30]. Applying a harmonic displacement  $u(h(r)) = \delta D e^{i\omega t}$  with  $\omega$  the pulsation, to the sphere, only resulted in complex values of the mechanical properties such as bulk and shear modulus in Eq. (5). The resolution of Eq. (8) gave the complex solution  $\tilde{\sigma}_z = \tilde{\Sigma} e^{i\omega t}$  with  $\tilde{\Sigma}$  the complex amplitude of the harmonic normal contact stress. The complex resulting force  $\Delta F_n$  was obtained using

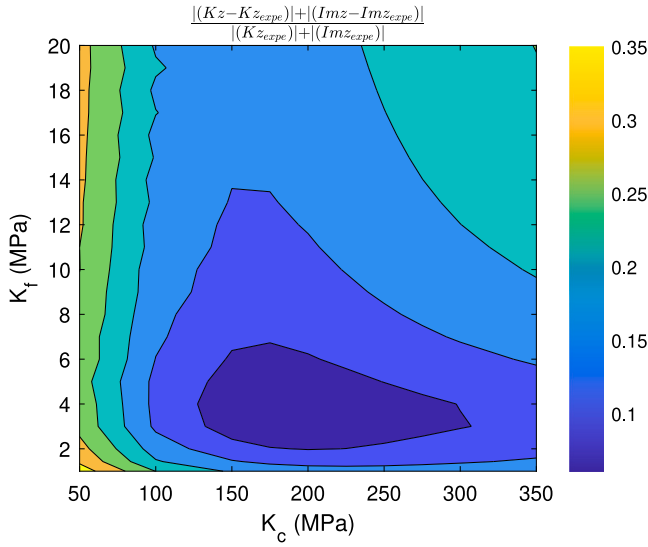


Fig. 5. Relative difference between numerical and experimental complex stiffness by varying bulk modulus  $K_c$  and  $K_f$  with  $G_c = 0.4$  MPa and  $\eta = 1.5$  mPa s under harmonic solicitation at a frequency of 38 Hz. Experimental data come from [4]. This relative difference is defined as:  $\frac{|Kz - Kz_{\text{expe}}| + |Imz - Imz_{\text{expe}}|}{|Kz_{\text{expe}}| + |Imz_{\text{expe}}|}$ .

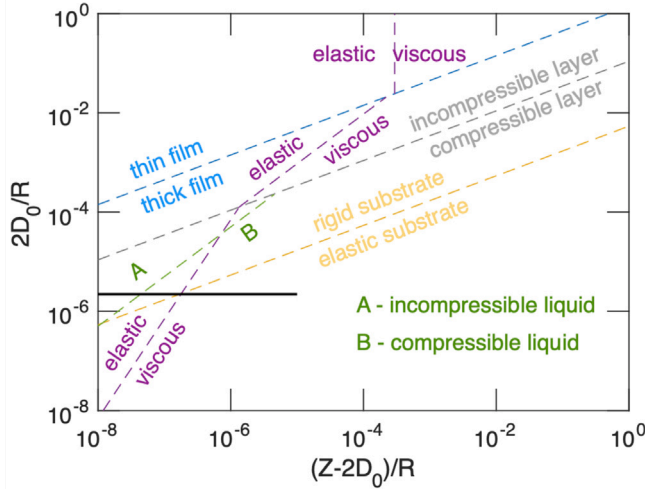


Fig. 6. Dynamic phase diagram for an adsorbed layer bulk modulus  $K_c = 200$  MPa and a fluid compressibility  $K_f = 4$  MPa. The dashed lines define the boundaries between different domains (i.e. thick/thin, incompressible/compressible and elastic/viscous films). The green dash and dotted lines are the boundaries below which the substrate compliance and fluid compressibility respectively play an important role in the contact complex stiffness. The formulations of these boundaries can be found in [26]. The continuous black line corresponds to the experimental case [4] with nanometric elaidic acid adsorbed layer on the surfaces separated by dodecane, with  $G_c = 0.4$  MPa,  $\eta = 1.5$  mPa s under harmonic solicitation at a frequency of 38 Hz.

Eq. (9). The stiffness  $Kz$  and damping  $Imz$  were then determined as the real and imaginary parts of the ratio between the complex resulting force  $\Delta F_n$  and the amplitude of the imposed harmonic solicitation  $\delta D$ :

$$Kz = \Re\left(\frac{\Delta F_n}{\delta D}\right) \quad \text{and} \quad Imz = \Im\left(\frac{\Delta F_n}{\delta D}\right) \quad (10)$$

where  $\Re(\bullet)$  and  $\Im(\bullet)$  signify the real and imaginary parts of  $\bullet$  respectively.

### 3. Validation of the numerical model

The model was here confronted to both analytical and experimental results. The first validation was the classical case of a squeezed homogeneous incompressible film with rigid substrates, for which an analytical solution can be deduced. Then, a static contact between molecular layers on solid surfaces was modeled and compared with Hertz's theory. Finally, the model was validated in the dynamic case of a squeezed heterogeneous compressible film under harmonic solicitation by means of the prediction of experimental data from the literature: a first example of identification of the adsorbed layers mechanical properties was illustrated.

#### 3.1. Homogeneous incompressible interfacial film

In the case of homogeneous incompressible film (bulk modulus  $K \rightarrow \infty$ ) squeezed between rigid substrates, Eq. (B.18) becomes:

$$-\frac{1}{r} \frac{d}{dr} \left( r L o(r) \frac{d\sigma_z}{dr} \right) = \delta D \quad (11)$$

The resolution of this equation with the boundary conditions in Eq. (B.19) gives the analytical solution [24]:

$$\sigma_z(r) = \frac{3GR\delta D}{h(r)^2} \quad (12)$$

Fig. 2a shows the normal contact stress calculated with our numerical model compared to the analytical solution (Eq. (12)) with a shear modulus  $G = 10$  MPa,  $\delta D = 0.4$  nm,  $Z = 4.2$  nm,  $R = 1.94$  mm. These values of oscillation amplitude, distance and sphere radius are consistent with experimental values [4], used later in the text for comparison/validation. It can be seen here that the solution obtained by the FE model superimposes on the analytical one. The relative difference is inferior to 1%. In addition, Fig. 2b highlights the strong influence of the film compressibility on the normal contact stress. For a near incompressible Poisson coefficient  $\nu$  which is very close to the level of incompressibility  $\nu_{max} = 0.5$ , the normal resulting contact force  $F_n$  decreases significantly in comparison with that obtained for an incompressible film  $F_n^{incompressible}$ . This confirms the key role of the film compressibility on the interface mechanical properties, as previously observed in [18].

#### 3.2. Static contact between two elastic molecular layers on the solid surfaces

In this section, we consider a static contact between two molecular layers of thickness  $D_o$ , adsorbed on solid surfaces. For the numerical model validation, the presence of adhesive forces was neglected. Assuming no deformation of these adsorbed layers i.e. a high compressibility  $K_c$ , according to Hertz's theory, the contact pressure  $\sigma_n$  is deduced using Eq. (13).

$$\sigma_n = \sigma_o \sqrt{1 - \frac{r^2}{a^2}} \quad \text{if} \quad r \leq a \quad (13)$$

where  $a$ ,  $\delta$  and  $\sigma_o$  are the contact radius, the static deformation of the solids and the maximum pressure respectively.

$$a = \left( \frac{3F_n R}{2E'} \right)^{1/3} ; \quad \delta = \frac{a^2}{R} \quad \text{and} \quad \sigma_o = \frac{2aE'}{\pi R} \quad (14)$$

Numerically, we set the radius of the sphere  $R = 1.94$  mm and an identical thickness  $D_o = 2.1$  nm on each surface, both values taken from [4]. The sphere moves incrementally with a displacement of  $D_o/1000$  as described in Section 2.3.

Firstly, in order to compare the model with Hertz theory, we assumed that the adsorbed layers have the same mechanical properties as those of the solids (sphere and plane). The resulting contact force and the normal stress distribution corresponding to the force maximal value were close to those obtained with Hertz solution as shown in Fig. 3a and b, despite of fluctuations due to the explicit approach.

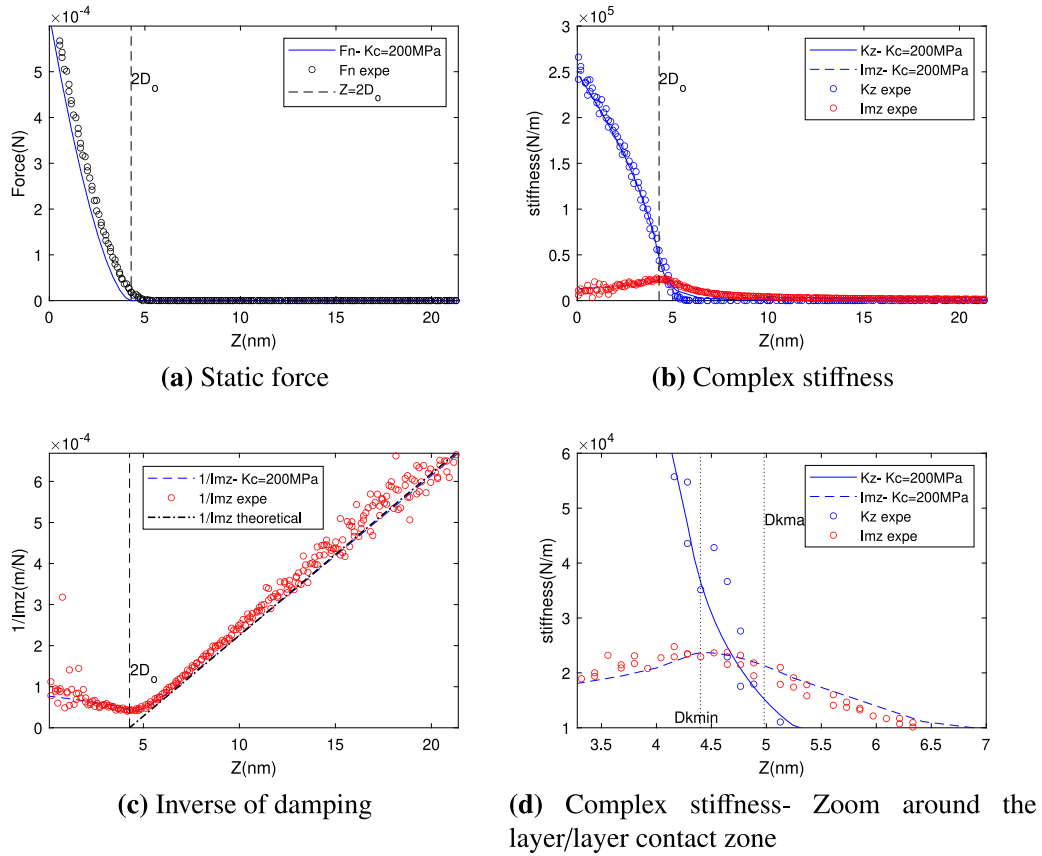


Fig. 7. Normal force, stiffness and inverse of damping evolution with  $K_c = 200$  MPa,  $G_c = 0.4$  MPa,  $\eta = 1.5$  mPa s and  $K_f = 4$  MPa under harmonic solicitation at a frequency of 38 Hz. Experimental data come from [4].

Secondly, to focus on the effects related to the compressibility of molecular layers, we set an identical shear modulus  $G_c = 0.4$  MPa for the molecular layers, taken from [4] as an example, and we varied their bulk modulus  $K_c$ . Fig. 4 shows the resulting contact force, normal stress and the surface separation distance numerically calculated for different bulk modulus compared to the Hertz' theory predictions. For low bulk modulus, for instance  $K_c = 100$  MPa, the contact force and the normal stress are smaller than those obtained from Hertz' theory while the contact dimension is larger. By increasing the bulk modulus  $K_c$ , the difference between the FE solution and Hertz' solution decreases. We can observe the increase in normal contact stress as well as the decrease in the contact zone dimension. For a very high bulk modulus,  $K_c = 10000$  MPa, meaning that the behavior of the layer is in the nearly incompressible domain, the solution is close to that obtained with Hertz' theory. These observations were also confirmed for the evolution of the distance between solid surfaces as shown in Fig. 4c. For a very high bulk modulus, the thickness of the molecular layers in the effective contact zone is almost equal to their initial thickness. This indicates that there is no deformation of these layers and the elastic deformation of the solids is predominant compared to that of the molecular layers. These conclusions were in agreement with experimental findings in [4]. Thanks to these results, it can be concluded that this model is rather robust for the modeling of the squeezing of both compressible and incompressible thin layers.

### 3.3. Squeeze of an heterogeneous thin film under harmonic solicitation

The numerical model allowed one to predict the evolution of the stiffness, of the damping and of the static normal force when a harmonic displacement of small amplitude  $\delta D$  and pulsation  $\omega$  is superimposed on the sphere. The thin fluid film has thus a complex shear

modulus [48]:

$$G_f(i\omega) = i\eta\omega. \quad (15)$$

In order to fully validate our model, literature data from [4] were used, leading to  $G_c = 0.4$  MPa for the elaidic acid adsorbed layer of thickness  $D_o = 2.1$  nm and to a viscosity  $\eta = 1.5$  mPa s for the dodecane with  $R = 1.94$  mm, a frequency of 38 Hz and  $\delta D = 0.45$  nm. With these known parameters, the full comparison between experimental data and numerical results required to adjust the two only remaining parameters: the compressibility of the dodecane,  $K_f$ , and the bulk modulus of the adsorbed layer,  $K_c$ . This adjustment was performed by minimizing the relative difference between numerical and experimental complex stiffness as shown in Fig. 5. This led to an optimal couple  $K_c \approx 200$  MPa and  $K_f \approx 4$  MPa.

The validity of our assumptions was also checked by plotting the dynamic phase diagram issued from [26] for bulk modulus  $K_c = 200$  MPa and fluid compressibility  $K_f = 4$  MPa. Fig. 6 shows that the considered experimental case with nanometric adsorbed layers is almost situated in the compressible thin film domain together with the important influence of the substrate compliance and fluid compressibility. So, the assumptions made in the adopted model (film compressibility with substrate compliance) are still valid.

A final comparison between numerical and experimental data was performed. Fig. 7 shows the corresponding normal static force, the stiffness and the damping variation with the position of the sphere  $Z$  at a frequency of 38 Hz. For  $Z \gg 2D_o$  that is to say when no contact between adsorbed layers occurred, as shown in Fig. 7c the numerical reciprocal of the damping was equal to the theoretical one, which is a linear function of the surface separation distance  $Z$  (Eq. (16)), as expected at large separation distances [2,21].

$$1/mz_t = \frac{6\pi\eta R^2\omega}{Z - 2L_H} \quad (16)$$

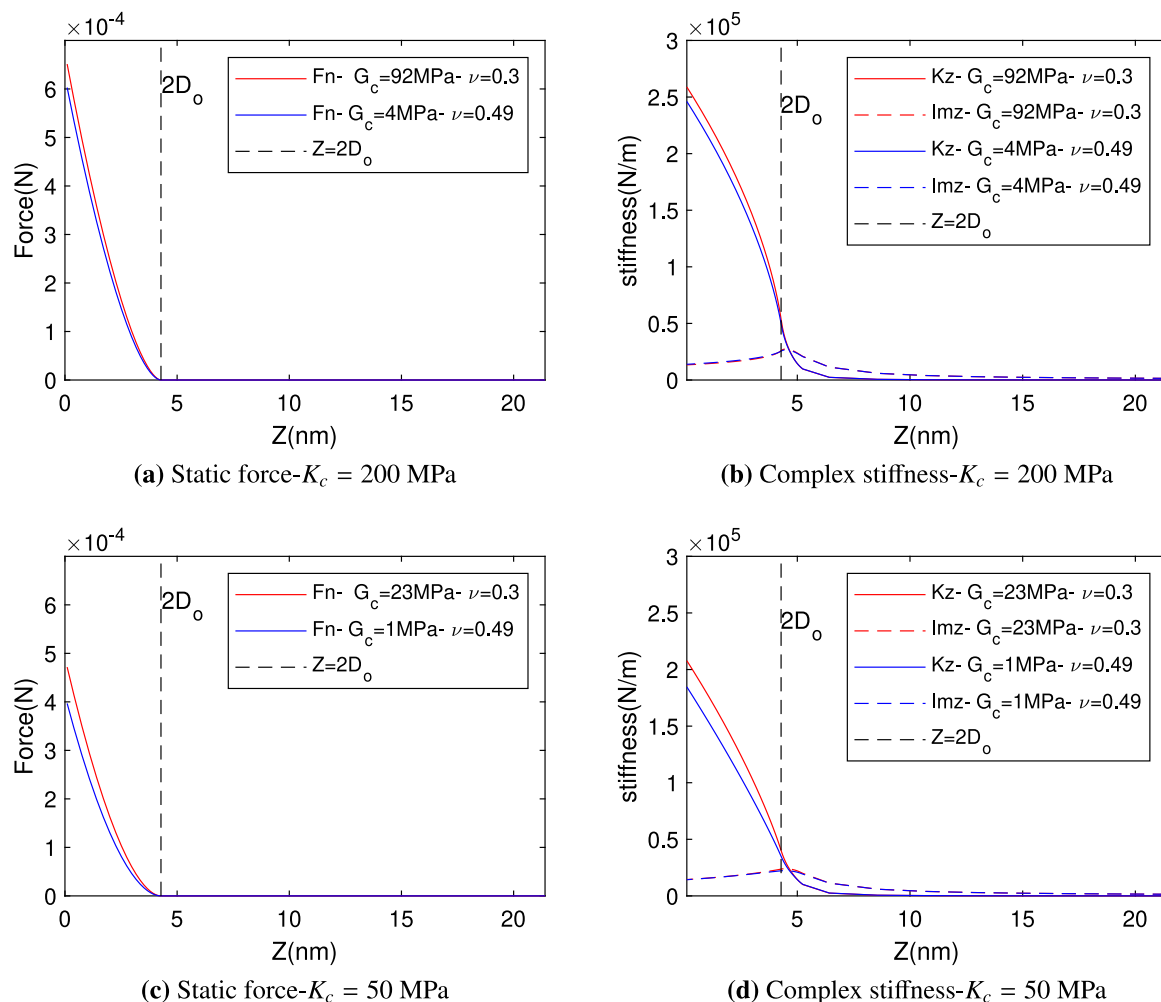


Fig. 8. Normal force, stiffness and damping evolution for different  $G_c$  with  $K_c = 200$  MPa (a and b) and  $K_c = 50$  MPa (respectively c and d), for  $\eta = 1.5$  mPa s and  $K_f = 5$  MPa under harmonic solicitation at a frequency of 38 Hz.

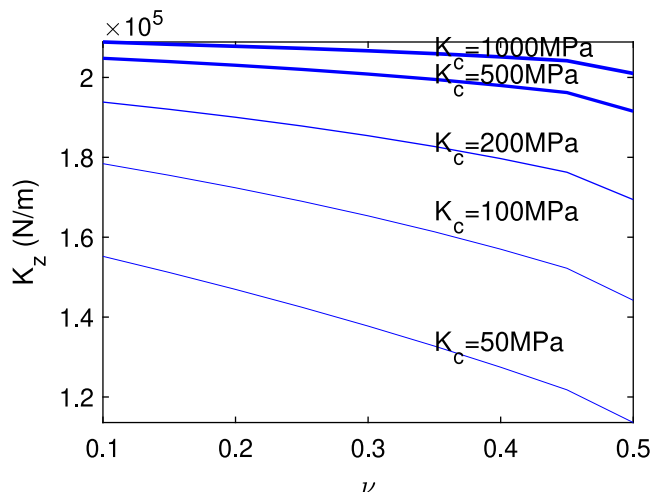


Fig. 9. Stiffness at  $Z = D_o$  for different  $K_c$  and  $\nu$  with  $\eta = 1.5$  mPa s and  $K_f = 5$  MPa under harmonic solicitation at a frequency of 38 Hz.

with  $L_H = D_o$  for a dense adsorbed monolayer.

In addition, from the phase diagram plotted in Fig. 6, the separation distance  $Z$  defining the elastic/viscous transition was estimated from

$Dk_{min} = 2D_o + 0.12$  nm to  $Dk_{max} = 2D_o + 0.7$  nm for  $K_c$  in the range of 50–1000 MPa. Fig. 7d shows a zoom of the complex stiffness at distances around these values,  $Z \approx 2D_o$ , confirming the occurrence of the elastic/viscous transition ( $K_z > Im_z$ ) between  $Dk_{min}$  and  $Dk_{max}$ .

It is noteworthy that the identified bulk modulus  $K_c$  together with shear modulus  $G_c = 0.4$  MPa gives the Poisson ratio  $\nu \geq 0.499$  and Young modulus  $E \approx 1.2$  MPa. This nearly incompressible Poisson ratio confirmed that the elaidic acid absorbed layers are highly dense and stiff, limiting the interpenetration between monolayers [4,5].

#### 4. Towards a better understanding of the squeeze mechanisms

The numerical model was further used to discuss the squeeze mechanisms: the shear elastic modulus of the adsorbed layer as well as the fluid compressibility and fluid viscosity were numerically varied in the following parts. The effect of the oscillation frequency was also investigated.

##### 4.1. Dependence of the shear elastic modulus of the adsorbed layer

Fig. 8 shows the normal static force and complex stiffness that were calculated for different values of  $G_c$ , giving Poisson ratio of 0.3 and 0.49 for the adsorbed layers. Overall, with a smaller Poisson ratio (corresponding to a larger shear modulus), the static force and stiffness are larger. On the one hand, for the bulk modulus  $K_c = 200$  MPa, as shown in Fig. 8 a and b, the normal static force and complex

stiffness remain similar for both large and small separation distance  $Z$ , regardless of the value of  $G_c$  with a difference inferior to 2% for the largest value of  $K_z$ . This seems to indicate that for a very thin film with a large bulk modulus, the shear modulus of adsorbed layers has little impact on interfacial properties in the vertical direction. On the other hand, for a smaller bulk modulus  $K_c = 50$  MPa, as shown in Fig. 8 c and d, the influence of the shear modulus of adsorbed layers on the static force and stiffness is more visible with a difference that can reach 10% for the largest values of  $K_z$  and  $F_n$ . Thus, it can be concluded that the influence of the shear modulus on the contact properties cannot be ignored in the case of a squeezed thin film with a strong compressibility (small value of  $K_c$ ).

This evolution was summarized in the mapping shown in Fig. 9 where the complex stiffness at  $Z = D_o$  was calculated for different values of  $G_c$  with Poisson ratio varying from 0.1 to 0.49 for the adsorbed layers. We can see that the relative influence of the shear modulus  $G_c$  depends on the compressibility  $K_c$ . This also confirms the importance of measuring the tangential stiffness as in [12] to reduce the number of adjustable parameters in the identification of the mechanical properties.

#### 4.2. Role of the fluid compressibility

Fig. 10 shows a significant influence of the fluid bulk modulus on the complex contact stiffness of the interface, especially at short separation distances, before the onset of contact between the two adsorbed layers: the contact stiffness,  $K_z$  starts increasing before the distance reaches  $2D_o$  and the damping is also very sensitive to the fluid bulk modulus, as shown in Fig. 10b. The peak observed on the damping increases and its position shifts to larger separation distances with increasing fluid bulk modulus. As the distance decreases, this peak disappears due to the increase of the relative contribution of the adsorbed layers.

In addition, following a similar approach as developed in [26], one can model the force response by spring-and-dashpot in series, each element corresponding to the fluid compressibility, layer and substrate deformation as well as the fluid friction coefficient associated to the Reynolds force. The detail of this theoretical calculation can be found in Appendix C. The equivalent stiffness was then obtained for  $Z \gg 2D_o$  in Eq. (17).

$$K_{z_i} = 18\pi\eta^2 R^3 \omega^2 \left( \frac{1}{(Z - 2D_o)^2 K_f} + \frac{2D_o}{M_{od}(Z - 2D_o)^3} + \frac{\pi\sqrt{2}R}{E'(Z - 2D_o)^{5/2}} \right) \quad (17)$$

This shows that the role of the fluid compressibility is predominant at large distances  $Z \gg 2D_o$ . On the one hand, with rigid layer and substrates, the real stiffness tends to zero with an incompressible fluid ( $K_f \rightarrow \infty$ ). On the other hand, as shown in Fig. 10c, the numerical stiffness is close to the theoretical one at large distances, confirming once more the validity of the numerical model. This theoretical model can also be used to identify the fluid compressibility value.

#### 4.3. Role of the fluid viscosity and the oscillation frequency

In Fig. 11a and b, a significant influence of the fluid viscosity and the oscillation frequency on the complex contact stiffness of the interface can be seen with the viscosity varying from 3 to 100 mPa s and the oscillation frequency ranging from 38 to 220 Hz. The increase in the damping  $Im_z$  by increasing the fluid viscosity  $\eta$  or the oscillation frequency can be easily explained by Eq. (16). Nevertheless, it is interesting to observe here is that increasing the fluid viscosity and/or the oscillation frequency leads to increasing the contact stiffness,  $K_z$ , at both large and small separation distances. This can be attributed to the fluid complex shear modulus,  $G_f$ , as described in Eq. (15). The increase in fluid viscosity and/or frequency also results in a larger

distance at which the elastic/viscous transition ( $Kz > Imz$ ) occurs. This observation was supported by the dynamic phase diagram plotted for various  $\eta\omega$  in Fig. 11c.

These predicted evolutions can be successfully compared to experimental measurements. On the one hand, Fig. 12a presents the influence of the fluid viscosity, 1.5 mPa s for the dodecane and 24 mPa s for the polyalpha olefin fluid (PAO), separating stearic acid adsorbed layers at a fixed frequency of 38 Hz. On the other hand, Fig. 12b highlights the effect of the oscillation frequency from 10 to 110 Hz for elaidic acid boundary layers separated by hexadecane (viscosity of 3.4 mPa s).

## 5. Conclusions

A numerical model based on continuum mechanics was developed to predict the squeeze behavior of a confined thin film between solid surfaces in both static and dynamic situations with the presence of adsorbed boundary layers. To do so, we used the generalized oedometric Reynolds model [19,24] with thin film assumptions and elastic deformation of solids. Numerically, this was done thanks to an explicit approach of resolution with a small incremental descending step of the sphere towards the plane. This model was validated by confrontation to analytical and experimental results, especially for nanometric-thin boundary layers.

We showed that this model, integrating solid deformation and compressibility of the layer as well as the frequency dependence, was able to provide the mechanical properties of the thin adsorbed layers, in both viscous and elastic regimes, at large distances and under confined situations. The dependence of the shear elastic modulus of the adsorbed layers was discussed and the role of fluid compressibility was confirmed. In addition, we highlighted the equivalence between fluid viscosity and frequency in the mechanical response of the interface.

This model was based on assumptions such as pure elastic behavior of the adsorbed layers, constant mechanical properties regardless of the normal load. For more complex layers, this model can easily take into account the potential viscoelastic behavior as well as the non-linearities of the film mechanical properties. Moreover, this model can be further extended into a three-dimensional one by integrating the roughness of the solid surfaces.

#### CRedit authorship contribution statement

**Van-Vuong Lai:** Methodology, Numerical simulation, Validation, Formal analysis, Investigation, Writing – original draft, Review and editing. **Emilie Delplanque:** Experimental data, Writing – review and editing. **Francois Sidoroff:** Theoretical validation, Resources, Writing – review and editing. **Denis Mazuyer:** Validation, Formal analysis, Investigation, Resources, Writing – review and editing, Funding acquisition, Supervision. **Juliette Cayer-Barrioz:** Validation, Formal analysis, Investigation, Resources, Writing – review and editing, Funding acquisition, Supervision.

#### Declaration of competing interest

The authors declare that they have no known competing financial interests or personal relationships that could have appeared to influence the work reported in this paper.

#### Data availability

Data will be made available on request.

#### Funding

The present research work was supported by the Agency for the ecological transition ADEME (France) through the IMOTEP project.

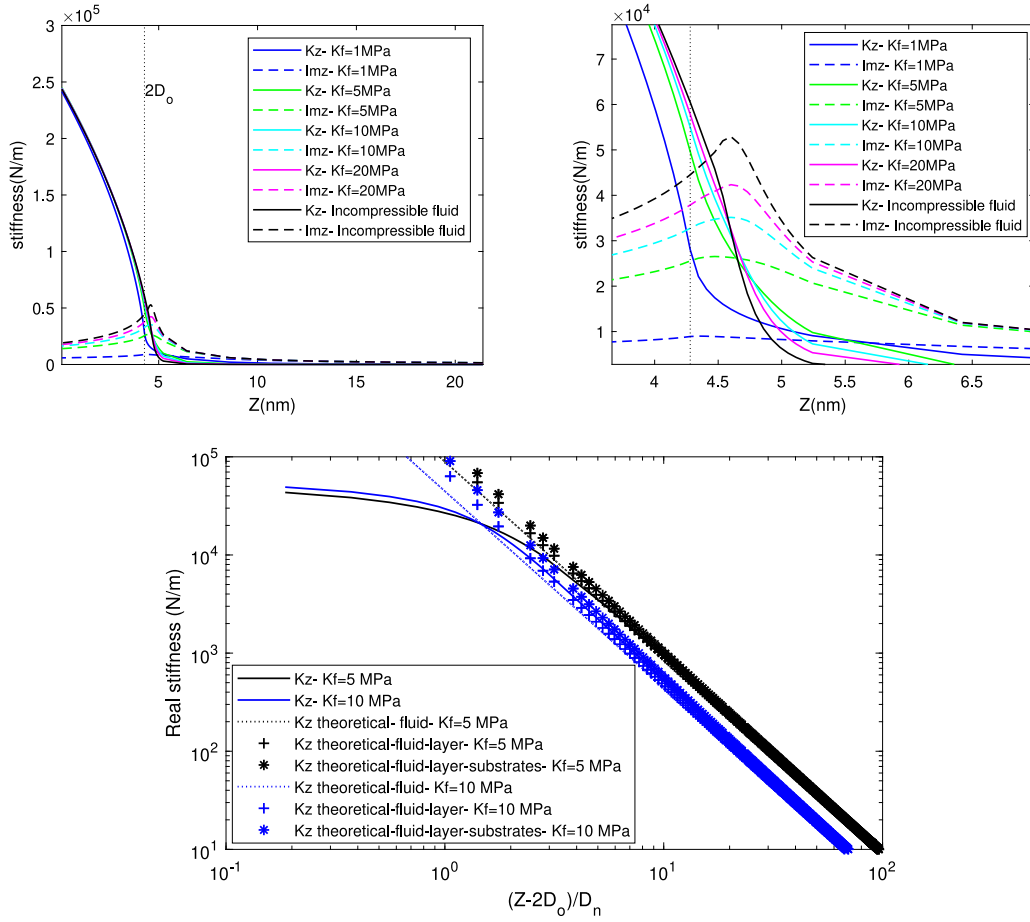


Fig. 10. (a) Normal stiffness and damping evolution for various fluid bulk modulus  $K_f$ .  $K_f$  was varied from 1 MPa to 20 MPa. (b) shows a zoom of stiffness and damping at small separation distances. (c) stiffness evolution compared to the theoretical value using Eq. (17) with  $D_n = \sqrt{(8\eta\omega 2D_o R/M_{ad})}$ . Results are obtained with shear modulus  $G_c = 0.4$  MPa,  $K_c = 200$  MPa,  $R = 1.94$  mm and  $D_o = 2.1$  nm.

## Appendix A. Hydrodynamic force calculation

In the case of undeformed solid surfaces and with a constant fluid viscosity  $\eta$ , the hydrodynamic pressure (stress) on solid surfaces, when a sphere moves towards a plane with a velocity  $V_z$ , was given by Chan and Horn [16]:

$$p = \frac{-3\eta R V_z}{h^2} \quad (\text{A.1})$$

The total hydrodynamic force  $F_H$  is obtained by integrating the total stress on the sphere/plane surface, giving:

$$F_H = \int_0^R 2\pi r p dr = \frac{6\pi\eta R^2 V_z}{h} \quad (\text{A.2})$$

where  $h$  is the solid surface separation distance and  $R$  is the radius of the sphere.

In addition, the fluid viscosity can depend on the pressure [5]:

$$\eta = \eta_o \exp(\alpha p) \quad (\text{A.3})$$

where the pressure-viscosity coefficient  $\alpha = 22 \text{ GPa}^{-1}$  in the case of hydrocarbon fluids.

## Appendix B. Generalized oedometric Reynolds model for the squeeze of a heterogeneous thin film confined between a sphere and a plane

In the case of a very thin film, as in [24] assumptions are made as follows:

- Vertical stress is constant according to  $z$
- The terms  $\frac{\partial u_\alpha}{\partial z}$  are predominant in the calculation of the shear stresses, which allows to write:

$$\begin{cases} \tau_{12} = \tau_{21} = 0 \\ \tau_{23} = G(z)\partial u_2/\partial z \\ \tau_{13} = G(z)\partial u_1/\partial z \end{cases} \quad (\text{B.1})$$

As in [18,19,24], one uses the equation “debit” to establish the equation of the problem of the squeezed film. One denotes the debit:

$$q_\alpha = \int_0^h u_\alpha dz \quad \alpha \in \{1, 2\} \quad (\text{B.2})$$

and the quantity:

$$E_{\text{debit}} = \int_0^h \epsilon_{ii} dz = \int_0^h \epsilon_{\alpha\alpha} dz + \delta D \quad (\text{B.3})$$

By some mathematical manipulations, Auslender *et al.* [24] demonstrated that:

$$E_{\text{debit}} = q_{\alpha,\alpha} + \delta D \quad (\text{B.4})$$

On the other hand, by combining Eqs. (7) and (B.3), we have:

$$E_{\text{debit}} = \int_0^h \epsilon_{ii} dz = \int_0^h \frac{\sigma_{ii}}{3K(z)} dz = \int_0^h \frac{1}{K(z) + 4/3G(z)} dz \sigma_z = C_o \sigma_z \quad (\text{B.5})$$

where

$$C_o = \int_0^h \frac{1}{K(z) + 4/3G(z)} dz \quad (\text{B.6})$$

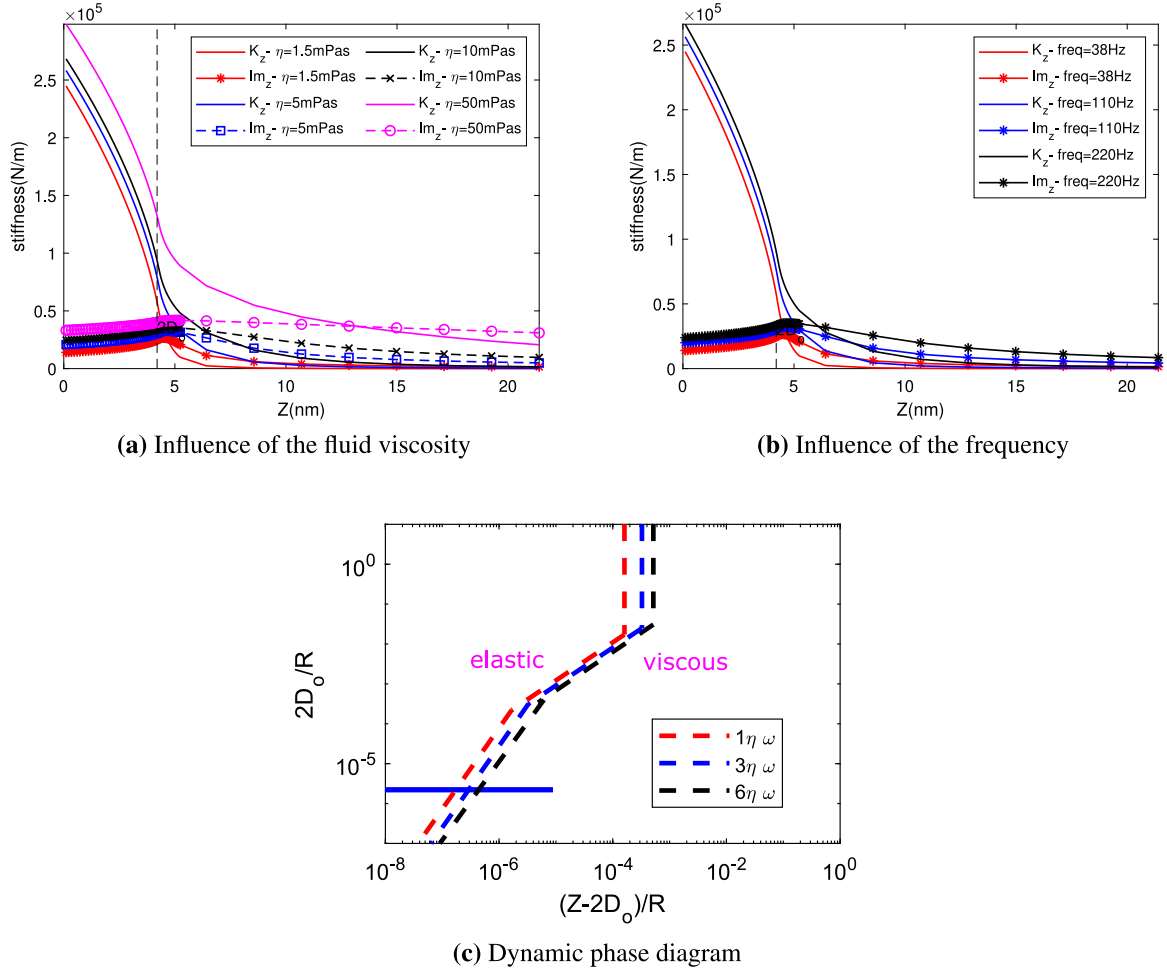


Fig. 11. Normal stiffness and damping evolution for various fluid viscosity  $\eta$  (a) and frequencies (b) as well as dynamic phase diagram for various  $\eta\omega$  (c). In (a)  $\eta$  was varied from 3mPas to 100 mPas with the frequency of 38 Hz. In (b) the frequency was varied from 38 to 220 Hz with the fluid viscosity of 1.5 mPa s. In (c), the dashed lines define the boundary between different domains (elastic/viscous films). The continuous line corresponds to the considered experimental and modeled conditions. These results were obtained with values of  $G_c = 0.4$  MPa,  $K_c = 200$  MPa,  $K_f = 5$  MPa,  $R = 1.94$  mm and  $D_o = 2.1$  nm.

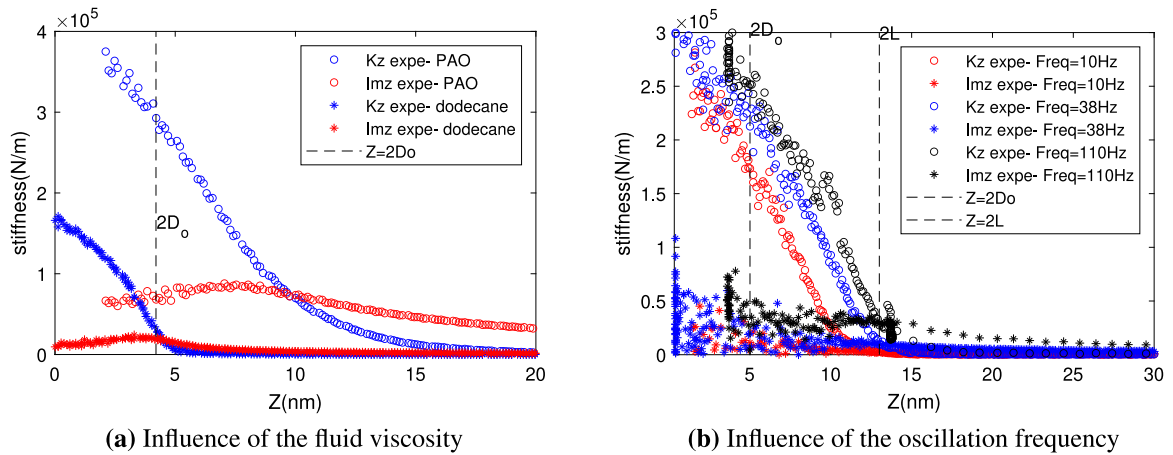


Fig. 12. Illustrative examples. Experimental evolution of the complex stiffness  $K_z$  and  $Im_z$  for stearic acid absorbed layers separated with different fluid viscosities (a) and for elaidic acid absorbed layers separated by hexadecane under different oscillation frequencies (b).

By applying the equation of equilibrium on the stress tensor Eq. (7) and by integration, we obtain:

and by integration, we obtain:

$$\gamma(z) \frac{\partial \sigma_z}{\partial x_\alpha} + \frac{\partial \tau_\alpha}{\partial z} = 0 \quad (B.7)$$

$$\tau_\alpha(z) = -\frac{\partial \sigma_z}{\partial x_\alpha} \int_0^z \gamma(y) dy + \tau_{\alpha 0} \quad (B.8)$$

By using Eq. (B.1), we have:

$$\frac{\partial u_\alpha}{\partial z} = -\frac{\partial \sigma_z}{\partial x_\alpha} \int_0^z \frac{\gamma(x)}{G(z)} dx + \frac{\tau_{ao}}{G(z)} \quad (B.9)$$

thus:

$$u_\alpha(z) = -\frac{\partial \sigma_z}{\partial x_\alpha} \int_0^z \frac{1}{G(y)} \int_0^y \gamma(x) dx dy + \tau_{ao} \int_0^z \frac{dy}{G(y)} + u_{ao} \quad (B.10)$$

By taking into account the boundary conditions Eq. (6), the displacement is obtained as:

$$u_\alpha(z) = \frac{\partial \sigma_z}{\partial x_\alpha} \left( \frac{I(h)}{J(h)} J(z) - I(z) \right) \quad (B.11)$$

where

$$\begin{cases} I(z) = \int_0^z \frac{1}{G(\epsilon)} \int_0^\epsilon \gamma(\zeta) d\zeta d\epsilon \\ J(z) = \int_0^z \frac{d\epsilon}{G(\epsilon)} \end{cases} \quad (B.12)$$

The integration of Eq. (B.11) gives:

$$q_\alpha = \int_0^h u_\alpha(z) dz = \frac{\partial \sigma_z}{\partial x_\alpha} \left( \frac{I(h)}{J(h)} \int_0^h J(z) dz - \int_0^h I(z) dz \right) = L_o \frac{\partial \sigma_z}{\partial x_\alpha} \quad (B.13)$$

where

$$L_o = \left( \frac{I(h)}{J(h)} \int_0^h J(z) dz - \int_0^h I(z) dz \right) \quad (B.14)$$

By replacing  $q_\alpha$  et  $E$  in Eq. (B.4), we obtain a partial differential equation:

$$C_o \sigma_z = \frac{\partial}{\partial x_\alpha} \left( L_o \frac{\partial \sigma_z}{\partial x_\alpha} \right) + \delta D \quad (B.15)$$

We can write Eq. (B.15) in the form:

$$C_o \sigma_z - \text{div}(L_o \text{grad} \sigma_z) = \delta D \quad (B.16)$$

and in the cylindrical coordinate system combining with the symmetry of revolution:

$$C_o(r) \sigma_z(r) - \frac{1}{r} \frac{d}{dr} \left( r L_o(r) \frac{d\sigma_z}{dr} \right) = \delta D \quad (B.17)$$

Assuming a relative elastic substrate deformation,  $w_r$ , at small separation distance, Eq. (8) was written as:

$$C_o(r) \sigma_z(r) - \frac{1}{r} \frac{d}{dr} \left( r L_o(r) \frac{d\sigma_z}{dr} \right) = \delta D - w_r \quad (B.18)$$

Eq. (B.18) was associated with the following boundary conditions:

$$\begin{aligned} \sigma_z|_{r=R} &= 0 \\ \frac{\sigma_z}{dr}|_{r=0} &= 0 \end{aligned} \quad (B.19)$$

Resolution of Eq. (B.18) was carried out thanks to FEM. By multiplying Eq. (B.18) by a test function  $P(r)$  and by partial integration in the domain  $[0, R]$ , we obtained the weak formulation of the problem:

$$\begin{aligned} \int_0^R r C_o \sigma_z P_r dr + \int_0^R \left( r L_o \frac{d\sigma_z}{dr} \frac{dP_r}{dr} \right) dr \\ = \int_0^R \delta D r P_r dr - \int_0^R \delta w_r r P_r dr \end{aligned} \quad (B.20)$$

By discretizing  $[0, R]$  in several finite elements, the approached solution was written as follows:

$$\sigma_z = \underline{N} \underline{\Sigma}_z \quad ; \quad P_r = \underline{N} \underline{P}_r \quad \text{and} \quad w_r = \underline{N} \underline{W}_r \quad (B.21)$$

where  $\underline{N}$  is the shape function vector. Here, the linear shape function was chosen for all elementary calculation.

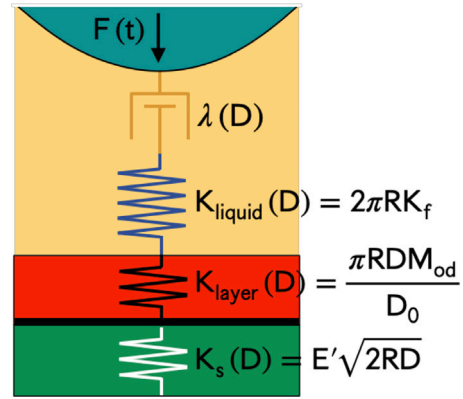


Fig. C.13. Schematic modeling of the fluid compressibility effect.  $\lambda(D)$  is the damping function of the liquid and  $K_{liquid}$  is its stiffness.

By substituting Eq. (B.21) in Eq. (B.20), we obtained:

$$\begin{aligned} \underline{P}_r^T \left( \int_0^R r C_o \underline{N}^T \underline{N} dr + \int_0^R \left( r L_o \frac{d\underline{N}^T}{dr} \underline{N} \frac{d}{dr} \right) dr \right) \underline{\Sigma}_z \\ = \underline{P}_r^T \int_0^R \delta D r \underline{N}^T dr - \underline{P}_r^T \int_0^R r \underline{N} \underline{W}_r \underline{N}^T dr \end{aligned} \quad (B.22)$$

We obtained the equation in a discretized form:

$$\underline{A} \underline{\Sigma}_z = \underline{B} - \underline{M} \underline{W}_r \quad (B.23)$$

where  $\underline{M} = \int_0^R r \underline{N}^T \underline{N} dr$  and  $\underline{W}_r = \underline{H} \underline{\Sigma}_z$ , with  $\underline{H}$  determined by the elastic half-space solution as in [19,49,50].

Thus, Eq. (B.23) became:

$$(\underline{A} + \underline{M} \underline{H}) \underline{\Sigma}_z = \underline{B} \quad (B.24)$$

$C_o$ ,  $L_o$  and integrals in Eqs. (B.6), (B.12), (B.14) and (B.22) were numerically computed using the function *trapz* in Matlab. As the film thickness at the center was very small compared to the sphere radius, the contact pressure is mainly localized around the center point,  $r = 0$ . Thus, the mesh size varied from  $h_o/1000$  around the center point,  $r = 0$ , up to  $h_o$  at  $r = R/20$ . This choice of mesh size was validated by comparing numerical results and analytical solutions.

### Appendix C. Theoretical contact stiffness at large distance with a compressible fluid

At large distance, the interface consists of a compressible liquid interacting with the substrate and the layer that are both considered as rigid materials. The interface was schematically modeled by the series combination of a viscous damper and springs associated to the liquid stiffness, the substrate stiffness and the layer stiffness, respectively, as shown in the following figure. In the remaining, distance  $D$  is defined as  $D = Z - 2D_0$  (see Fig. C.13).

In such case, the hydrodynamic force  $F_H$  due to the displacement amplitude  $h_0$  is simply:

$$F_H = \lambda(D) h_0 = \frac{6\pi\eta\omega h_0 R^2}{D} \quad (C.1)$$

It balances the elastic force due to the substrate deformation, the liquid and the layer compressibility. This force is  $K_t(D) \times \delta$ , where  $\delta$  is the elastic displacement of the liquid layer and  $K_t(D)$  is such as:

$$\frac{1}{K_t(D)} = \frac{1}{K_{liquid}(D)} + \frac{1}{K_{layer}(D)} + \frac{1}{K_s(D)} \quad (C.2)$$

Thus, it can be written:

$$\frac{\delta}{h_0} = \frac{6\pi\eta\omega R^2}{K_t(D) D} \quad (C.3)$$

At large distance, it is shown that the complex elastic modulus  $G(\omega)$  can be approximated [26] by:

$$G(\omega) \simeq i\omega\lambda(D) \left[ 1 - i \frac{\delta}{h_0} \right] \quad (\text{C.4})$$

It comes from the latter equation that the normal stiffness  $K_z(D)$  of the interface is:

$$K_z(D) = \text{Re}[G(\omega)] \simeq \frac{18\pi\eta^2\omega^2 R^3}{K_f D^2} \left[ 1 + \frac{2D_0}{D} \times \frac{K_f}{M_{od}} + \sqrt{\frac{2R}{D}} \times \frac{\pi K_f}{E'} \right] \quad (\text{C.5})$$

As at large distance ( $2D_0 \ll Z$ ), the terms proportional to  $1/D$  are much smaller than 1, it comes:

$$K_z(D) \simeq \frac{18\pi\eta^2\omega^2 R^3}{K_f D^2} \quad (\text{C.6})$$

## References

- [1] Lundgren SM, Ruths M, Danerlöv K, Persson K. Effects of unsaturation on film structure and friction of fatty acids in a model base oil. *J Colloid Interface Sci* 2008;326(2):530–6.
- [2] Cayer-Barrioz J, Mazuyer D, Tonck A, Yamaguchi E. Drainage of a wetting liquid: Effective slippage or polymer depletion? *Tribol Lett* 2008;32(2):81–90.
- [3] Levine O, Zisman W. Physical properties of monolayers adsorbed at the solid–air interface. I. Friction and wettability of aliphatic polar compounds and effect of halogenation. *J Phys Chem* 1957;61(8):1068–77.
- [4] Crespo A, Morgado N, Mazuyer D, Cayer-Barrioz J. Effect of unsaturation on the adsorption and the mechanical behavior of fatty acid layers. *Langmuir* 2018;34(15):4560–7.
- [5] Abouhadid F, Crespo A, Morgado N, Mazuyer D, Cayer-Barrioz J. Friction laws for saturated/unsaturated fatty acid layers. *Tribol Lett* 2021;69(2):1–10.
- [6] Campana M, Teichert A, Clarke S, Steitz R, Webster JR, Zarbakhsh A. Surfactant adsorption at the metal–oil interface. *Langmuir* 2011;27(10):6085–90.
- [7] Tadokoro C, Araya S, Okubo H, Nakano K, Sasaki S. Polarization observations of adsorption behavior of fatty acids using optical anisotropy of liquid crystal. *Tribol Lett* 2016;64(2):1–9.
- [8] Daillant J, Gibaud A. X-ray and neutron reflectivity: Principles and applications, Vol. 770. Springer; 2008.
- [9] Tabor D, Winterton RS. The direct measurement of normal and retarded van der Waals forces. *Proc R Soc Lond Ser A Math Phys Eng Sci* 1969;312(1511):435–50.
- [10] Tonck A. Développement d'un appareil de mesures de forces de surface et de nanorhéologie (Ph.D. thesis), Ecully, Ecole centrale de Lyon; 1989.
- [11] Tonck A, Georges J, Loubet J. Measurements of intermolecular forces and the rheology of dodecane between alumina surfaces. *J Colloid Interface Sci* 1988;126(1):150–63.
- [12] Crespo A, Mazuyer D, Morgado N, Tonck A, Georges J-M, Cayer-Barrioz J. Methodology to characterize rheology, surface forces and friction of confined liquids at the molecular scale using the ATLAS apparatus. *Tribol Lett* 2017;65(4):1–10.
- [13] Campen S, Green J, Lamb G, Spikes H. In situ study of model organic friction modifiers using liquid cell AFM: self-assembly of octadecylamine. *Tribol Lett* 2015;58(3):1–15.
- [14] Campen S, Green J, Lamb G, Spikes H. In situ study of model organic friction modifiers using liquid cell AFM; saturated and mono-unsaturated carboxylic acids. *Tribol Lett* 2015;57(2):1–20.
- [15] Cayer-Barrioz J, Mazuyer D, Tonck A, Yamaguchi E. Frictional rheology of a confined adsorbed polymer layer. *Langmuir* 2009;25(18):10802–10.
- [16] Chan DY, Horn R. The drainage of thin liquid films between solid surfaces. *J Chem Phys* 1985;83(10):5311–24.
- [17] Montfort J, Hadziioannou G. “Equilibrium” and dynamic behavior of thin films of a perfluorinated polyether. *J Chem Phys* 1988;88(11):7187–96.
- [18] Auslender F, Trifa M, Sidoroff F. Material compressibility effects for the squeeze of very thin films. *Eur J Mech A Solids* 1999;18(3):499–515.
- [19] Trifa M, Auslender F, Sidoroff F. Nanorheological analysis of the sphere plane contact problem with interfacial films. *Internat J Engrg Sci* 2002;40(2):163–76.
- [20] Movchan AB, Rebrov KR, Rodin GJ. Axisymmetric deformation of compressible, nearly incompressible, and incompressible thin layers between two rigid surfaces. *Int J Solids Struct* 2021;214:61–73.
- [21] Georges J, Millot S, Loubet J, Tonck A. Drainage of thin liquid films between relatively smooth surfaces. *J Chem Phys* 1993;98(9):7345–60.
- [22] Delamarre S, Gmür T, Spencer ND, Cayer-Barrioz J. Polymeric friction modifiers: Influence of anchoring chemistry on their adsorption and effectiveness. *Langmuir* 2022;38(37):11451–8.
- [23] Mazuyer D, Tonck A, Cayer-Barrioz J. Friction control at the molecular level: from superlubricity to stick-slip. In: *Superlubricity*. Elsevier; 2007, p. 397–426.
- [24] Auslender F, Sidoroff F. Nanorheological behaviour of confined liquid layers for normal contact. *Tribol Ser* 1996;31:195–204.
- [25] Trifa M. Nanorhéologie du contact sphère-plan avec couche mince interfaciale (Ph.D. thesis), Ecully, Ecole centrale de Lyon; 1999.
- [26] Leroy S, Charlaix E. Hydrodynamic interactions for the measurement of thin film elastic properties. *J Fluid Mech* 2011;674:389–407.
- [27] Hocking LM. The effect of slip on the motion of a sphere close to a wall and of two adjacent spheres. *J Eng Math* 1973;7(3):207–21.
- [28] Gacoin E, Frétygn C, Chateauinois A, Perriot A, Barthel E. Measurement of the mechanical properties of thin films mechanically confined within contacts. *Tribol Lett* 2006;21(3):245–52.
- [29] Mazuyer D, Cayer-Barrioz J, Tonck A, Jarnias F. Friction dynamics of confined weakly adhering boundary layers. *Langmuir* 2008;24(8):3857–66.
- [30] Auslender F. Nanorhéologie des couches minces confinées application aux appareils à forces de surface (Ph.D. thesis), Ecully, Ecole centrale de Lyon; 1996.
- [31] Johnson KL, Kendall K, Roberts a. Surface energy and the contact of elastic solids. *Proc R Soc Lond Ser A Math Phys Eng Sci* 1971;324(1558):301–13.
- [32] Barthel E, Perriot A, Chateauinois A, Frétygn C. Elastic contact to nearly incompressible coatings: Stiffness enhancement and elastic pile-up. *Phil Mag* 2006;86(33–35):5359–69.
- [33] Barthel E. Adhesive contact of a compliant sphere to an elastic coated substrate: the thin film limit. *J Adhes* 2007;83(8):729–39.
- [34] Chen J, Bull S. Finite element analysis of contact induced adhesion failure in multilayer coatings with weak interfaces. *Thin Solid Films* 2009;517(13):3704–11.
- [35] Djabella H, Arnell R. Finite element analysis of elastic stresses in multilayered systems. *Thin Solid Films* 1994;245(1–2):27–33.
- [36] Sridhar I, Zheng Z, Johnson K. A detailed analysis of adhesion mechanics between a compliant elastic coating and a spherical probe. *J Phys D: Appl Phys* 2004;37(20):2886.
- [37] Kot M. Contact mechanics of coating-substrate systems: Monolayer and multilayer coatings. *Arch Civ Mech Eng* 2012;12(4):464–70.
- [38] Assogba OC, Tan Y, Zhou X, Zhang C, Anato JN. Numerical investigation of the mechanical response of semi-rigid base asphalt pavement under traffic load and nonlinear temperature gradient effect. *Constr Build Mater* 2020;235:117406.
- [39] Yu C, Wang Z, Wang QJ. Analytical frequency response functions for contact of multilayered materials. *Mech Mater* 2014;76:102–20.
- [40] Zhang J, Wang T, Zhang C, Wang L, Ma X, Yin L, et al. A two-dimensional contact model between a multilayered solid and a rigid cylinder. *Surf Coat Technol* 2019;360:382–90.
- [41] Wallace ER, Chaise T, Nelias D. Rolling contact on a viscoelastic multi-layered half-space. *Int J Solids Struct* 2022;239:111388.
- [42] Nikravesh S, Ryu D, Shen Y-L. Instabilities of thin films on a compliant substrate: direct numerical simulations from surface wrinkling to global buckling. *Sci Rep* 2020;10(1):1–19.
- [43] Doig M, Warrens CP, Camp PJ. Structure and friction of stearic acid and oleic acid films adsorbed on iron oxide surfaces in squalane. *Langmuir* 2014;30(1):186–95.
- [44] Cui S, Cummings P, Cochran H. Molecular simulation of the transition from liquidlike to solidlike behavior in complex fluids confined to nanoscale gaps. *J Chem Phys* 2001;114(16):7189–95.
- [45] Fang T-H, Wu J-H. Molecular dynamics simulations on nanoindentation mechanisms of multilayered films. *Comput Mater Sci* 2008;43(4):785–90.
- [46] Peng P, Liao G, Shi T, Tang Z, Gao Y. Molecular dynamic simulations of nanoindentation in aluminum thin film on silicon substrate. *Appl Surf Sci* 2010;256(21):6284–90.
- [47] Mayo SL, Olafson BD, Goddard WA. DREIDING: A generic force field for molecular simulations. *J Phys Chem* 1990;94(26):8897–909.
- [48] Zwanzig R, Mountain RD. High-frequency elastic moduli of simple fluids. *J Chem Phys* 1965;43(12):4464–71.
- [49] Yang P, Wen S. Pure squeeze action in an isothermal elastohydrodynamically lubricated spherical conjunction Part 1. Theory and dynamic load results. *Wear* 1991;142(1):1–16.
- [50] Larsson R, Hoglund E. Numerical simulation of a ball impacting and rebounding a lubricated surface. *Int J Multiph Flow* 1996;22(S1):148–9.